

IDCS J1426.5+3508: THE MOST MASSIVE GALAXY CLUSTER AT $Z > 1.5$

MARK BRODWIN¹, MICHAEL McDONALD², ANTHONY H. GONZALEZ³, S. A. STANFORD^{4,5}, PETER R. EISENHARDT⁶,
DANIEL STERN⁶ & GREGORY R. ZEIMANN⁷

Draft version April 8, 2015

ABSTRACT

We present a deep (100 ks) *Chandra* observation of IDCS J1426.5+3508, a spectroscopically confirmed, infrared-selected galaxy cluster at $z = 1.75$. This cluster is the most massive galaxy cluster currently known at $z > 1.5$, based on existing Sunyaev-Zeldovich (SZ) and gravitational lensing detections. We confirm this high mass via a variety of X-ray scaling relations, including T_X - M , f_g - M , Y_X - M , and L_X - M , finding a tight distribution of masses from these different methods, spanning $M_{500} = 2.3\text{--}3.3 \times 10^{14} M_\odot$, with the low-scatter Y_X -based mass $M_{500, Y_X} = 2.6^{+1.5}_{-0.5} \times 10^{14} M_\odot$. IDCS J1426.5+3508 is currently the only cluster at $z > 1.5$ for which X-ray, SZ and gravitational lensing mass estimates exist, and these are in remarkably good agreement. We find a relatively tight distribution of the gas-to-total mass ratio, employing total masses from all of the aforementioned indicators, with values ranging from $f_{gas,500} = 0.087\text{--}0.12$. We do not detect metals in the ICM of this system, placing a 2σ upper limit of $Z(r < R_{500}) < 0.18 Z_\odot$. This upper limit on the metallicity suggests that this system may still be in the process of enriching its intracluster medium. The ICM has a dense, low-entropy core, offset by ~ 30 kpc from the X-ray centroid, which makes it one of the few “cool core” clusters discovered at $z > 1$, and the first known cool core cluster at $z > 1.2$. The offset of this core from the large-scale centroid suggests that this cluster has had a relatively recent ($\lesssim 500$ Myr) merger/interaction with another massive system.

Subject headings: galaxies: clusters: individual (IDCS J1426.5+3508) — galaxies: clusters: intracluster medium — galaxies: high-redshift — large scale structure of universe — X-rays: galaxies: clusters

1. INTRODUCTION

In recent years the study of galaxy clusters has meaningfully entered the $z > 1$ regime, with several surveys identifying large samples via X-ray (Fassbender et al. 2011; Mehrrens et al. 2012), Sunyaev-Zel’dovich (SZ, Bleem et al. 2015; Hasselfield et al. 2013; Planck Collaboration et al. 2015), infrared (IR, Eisenhardt et al. 2008; Muzzin et al. 2009; Papovich et al. 2010; Rettura et al. 2014) and radio (Wylezalek et al. 2013; Blanton et al. 2014) selections. These surveys have extended the reach of cluster cosmology (e.g., Benson et al. 2013), scaling relations (e.g., Andersson et al. 2011) and galaxy formation and evolution in the richest environments (e.g., Tran et al. 2010; Hilton et al. 2010; Brodwin et al. 2013) to $z \sim 1.5$.

It is crucial to identify the earliest massive progenitors of these $1 \lesssim z \lesssim 1.5$ cluster samples, and the present-day massive clusters into which they evolve, in order to quantify the build-up of the intracluster medium (ICM) and the establishment of self-similarity. In particular,

the scaling relations between different cluster mass observables — e.g., ICM temperature, SZ signal, weak lensing — are calibrated to better than $\sim 20\%$ at $z < 0.5$ (e.g., Kravtsov et al. 2006; Vikhlinin et al. 2009b; Andersson et al. 2011), but are currently poorly constrained at high redshifts ($z > 1$) where clusters provide the greatest leverage as probes of the growth of structure.

Very massive, high redshift galaxy clusters also provide a natural testing ground to confirm or refute the predictions stemming from recent galaxy evolution studies in clusters at $1 \lesssim z \lesssim 1.5$. While little star formation activity is seen in the most massive ($M \sim 10^{15} M_\odot$) South Pole Telescope (SPT) clusters in this regime (e.g., Brodwin et al. 2010; Foley et al. 2011; Stalder et al. 2013), the case is notably different for clusters with masses in the range $M \sim (1 - 4) \times 10^{14} M_\odot$. Indeed, Brodwin et al. (2013) reported the discovery of a major epoch of star formation at $z \gtrsim 1.4$ for IRAC Shallow Cluster Survey (ISCS) clusters in this mass range. They attributed it in part to a high merging rate of gas-rich cluster members, as suggested by Mancone et al. (2010). A consequence of this model is that the epoch at which the merging (and hence merger-induced star formation) ceases should be a function of cluster mass. While the SPT clusters at $z \lesssim 1.3$ are generally too massive to permit efficient merging, their lower-mass progenitors at higher redshifts should have the high star formation rates seen in the ISCS. Indeed, in the most distant SPT cluster, SPT-CL J2040-4451, with a mass of $M_{500, SZ} \sim 3.2 \times 10^{14} M_\odot$ at $z = 1.48$, residual star formation activity still persists after its earlier bursting phase (Bayliss et al. 2014)

To extend the infrared cluster search to $z > 1.5$, we

¹ Department of Physics and Astronomy, University of Missouri, Kansas City, MO 64110

² Kavli Institute for Astrophysics and Space Research, Massachusetts Institute of Technology, Cambridge, MA 02139

³ Department of Astronomy, University of Florida, Gainesville, FL 32611

⁴ Department of Physics, University of California, Davis, CA 95616

⁵ Institute of Geophysics and Planetary Physics, Lawrence Livermore National Laboratory, Livermore, CA 94551

⁶ Jet Propulsion Laboratory, California Institute of Technology, Pasadena, CA 91109

⁷ Department of Astronomy and Astrophysics, Pennsylvania State University, University Park, Pennsylvania 16802

repeated the methodology of the ISCS using the *Spitzer* Deep, Wide-Field Survey (SDWFS, Ashby et al. 2009), which quadrupled the *Spitzer*/IRAC exposure time over the 9 deg² IRAC Shallow Survey (Eisenhardt et al. 2004). The resulting survey, the IRAC Distant Cluster Survey (IDCS, Stanford et al. 2012; Brodwin et al. 2012; Gonzalez et al. 2012), has identified two of the most distant clusters to date: IDCS J1426.5+3508 at $z = 1.75$ (Stanford et al. 2012) and IDCS J1433.2+3306 at $z = 1.89$ (Zeimann et al. 2012). The latter appears to be a moderate mass cluster still in the process of formation, whereas IDCS J1426.5+3508 at $z = 1.75$, the subject of this paper, is a very massive cluster.

Stanford et al. (2012) reported a detection in only 8.3 ks of archival *Chandra* X-ray Observatory data, resulting in an L_X -based mass estimate of $M_{500, L_X} = (3.3 \pm 1.0) \times 10^{14} M_\odot$ ⁸. IDCS J1426.5+3508 was also observed with the Sunyaev–Zeldovich Array (SZA), a subarray of the Combined Array for Research in Millimeter-wave Astronomy (CARMA). An SZ-based mass of $M_{500, SZ} = (2.6 \pm 0.7) \times 10^{14} M_\odot$ was measured from the strong (5.3σ) decrement (Brodwin et al. 2012). Finally, IDCS J1426.5+3508 has a giant gravitational arc, from which a minimum mass of $M_{500, \text{arc}} \gtrsim 2.0 \times 10^{14} M_\odot$ was estimated (Gonzalez et al. 2012). Although these independent mass measurements are all in good agreement, indicating that IDCS J1426.5+3508 is a very massive, relaxed cluster at $z = 1.75$, the L_X -based X-ray mass was based on only 53 counts and is highly uncertain.

In this paper we present deep new *Chandra* observations from which we measure the ICM properties of IDCS J1426.5+3508. In §2 we describe the data used in this analysis. In §3 we present the flux, energy spectrum and gas density profile of IDCS J1426.5+3508, along with the quantities we derive from these direct measurements, including the luminosity, temperature, gas mass and metallicity. Using standard scaling relations from the literature, we estimate M_{500} for IDCS J1426.5+3508 from four different X-ray estimators in §4, and compare these to complementary SZ- and lensing-based mass estimates. We also compute gas fractions for each of these halo mass estimates and compare these with the value predicted from low-redshift clusters. In §5 we place IDCS J1426.5+3508 in the context of the known $z > 1.5$ galaxy cluster population and discuss the evolutionary state of its ICM. Finally, we present our conclusions in §6. We use $\Omega_m = 0.27$, $\Omega_\Lambda = 0.73$ and $H_0 = 70 \text{ km s}^{-1} \text{ Mpc}^{-1}$ throughout.

2. DATA

The X-ray data used in this work were acquired via *Chandra* proposal 148000534 (PI: Brodwin). A total exposure of 100 ks was acquired over two pointings (OBSIDs 15168 and 16321). This exposure time was chosen to obtain 500 X-ray source counts, but due to the evolving effective area at low energies (Marshall et al. 2004; O’Dell et al. 2013) we obtained slightly fewer than anticipated. The data, obtained with ACIS-I, were cleaned for background flares before applying the latest calibration corrections using CIAO v4.6 and CALDB v4.6.1.1.

⁸ $M_{\Delta, A}$ refers to the mass within r_Δ , the radius at which the mean overdensity is Δ times the critical density, as inferred via mass proxy A.

3. X-RAY PROPERTIES OF IDCS J1426.5+3508

3.1. Images, Centroid and Peak

Chandra and *HST* images of IDCS J1426.5+3508 are shown in Figure 1. The first column shows *Chandra* images and contours for Gaussian-smoothed (FWHM = 3", upper panel) and adaptively smoothed (lower panel) 0.5–2.0 keV X-ray images, respectively. The 2nd column shows these contours overlaid on color optical/IR *HST* images, a full description of which are given in (Mo et al. in prep.). The upper right panel is zoomed in to the cluster core to better show the brightest cluster galaxy (BCG) and the giant gravitational arc.

We use the centroid measured within a 250–500 kpc annulus as the cluster center, which tends to provide less biased estimates of the global properties for unrelaxed clusters. This choice of center, $(\alpha_X, \delta_X) = (14:26:32.6, +35:08:25)$, is within 4" of the X-ray peak, within 5" of the BCG position (Stanford et al. 2012) and within 28" of the SZ centroid (Brodwin et al. 2012). Given the uncertainty in the SZ centroid ($\approx 35''$), this positional offset is not statistically significant.

3.2. Point Sources

Point sources were identified and masked using an automated routine following the wavelet decomposition technique described in Vikhlinin et al. (1998). There are two bright X-ray point source near the cluster core, previously discussed in Stanford et al. (2012). The northern one is a QSO in the cluster, with a flux of $S_{0.5-2} \approx 1.85_{-0.37}^{+0.33} \times 10^{-15} \text{ erg s}^{-1} \text{ cm}^{-2}$. The southern one is a bright radio source listed in both the NVSS (Condon et al. 1998) and FIRST (Becker et al. 1995) catalogs. It has a flux of $\sim 95 \text{ mJy}$ at 1.4 GHz, and was found to have a 31 GHz flux of $5.3 \pm 0.3 \text{ mJy}$ in the SZ analysis of Brodwin et al. (2012). Here we measure a flux of $S_{0.5-2} \approx 5.68_{-0.69}^{+0.71} \times 10^{-15} \text{ erg s}^{-1} \text{ cm}^{-2}$. These point sources, along with several others at larger clustercentric radii, are masked and do not affect this analysis.

3.3. Counts, Flux and Luminosity

We measure 401 net counts (0.5–6 keV) from IDCS J1426.5+3508, after point source masking and background subtraction. The flux in the soft band is $S_{0.5-2} = (2.2 \pm 0.6) \times 10^{-14} \text{ erg s}^{-1} \text{ cm}^{-2}$, corresponding to a luminosity of $L_{0.5-2} = (3.6 \pm 0.5) \times 10^{44} \text{ erg s}^{-1}$. The bolometric luminosity over the 0.01–100 keV energy range is measured from the best-fit model described below (§3.4) to be $L_{X, \text{bol}} = (12.8 \pm 1.1) \times 10^{44} \text{ erg s}^{-1}$. These quantities are all measured within $r_{500, Y_X} = 530 \pm 10 \text{ kpc}$, as determined from the core-excised Y_X measurement described below (§3.6). Pratt et al. (2009) showed the bolometric luminosity to be a lower scatter mass proxy than $L_{0.5-2}$. Using their scaling relation, we find $M_{500, L_X, \text{bol}} = (2.8 \pm 0.3) \times 10^{14} M_\odot$.

3.4. Temperature

The 0.5–6.0 keV ACIS-I spectra within r_{2500} ($\sim 0.45 r_{500, Y_X}$; Vikhlinin et al. 2006) for each OBSID are shown in Figure 2. This aperture was chosen to maximize signal to noise, although we also consider a core-excised (0.15–1) r_{500} annulus below. The spectroscopic temperature was measured by modeling the X-ray

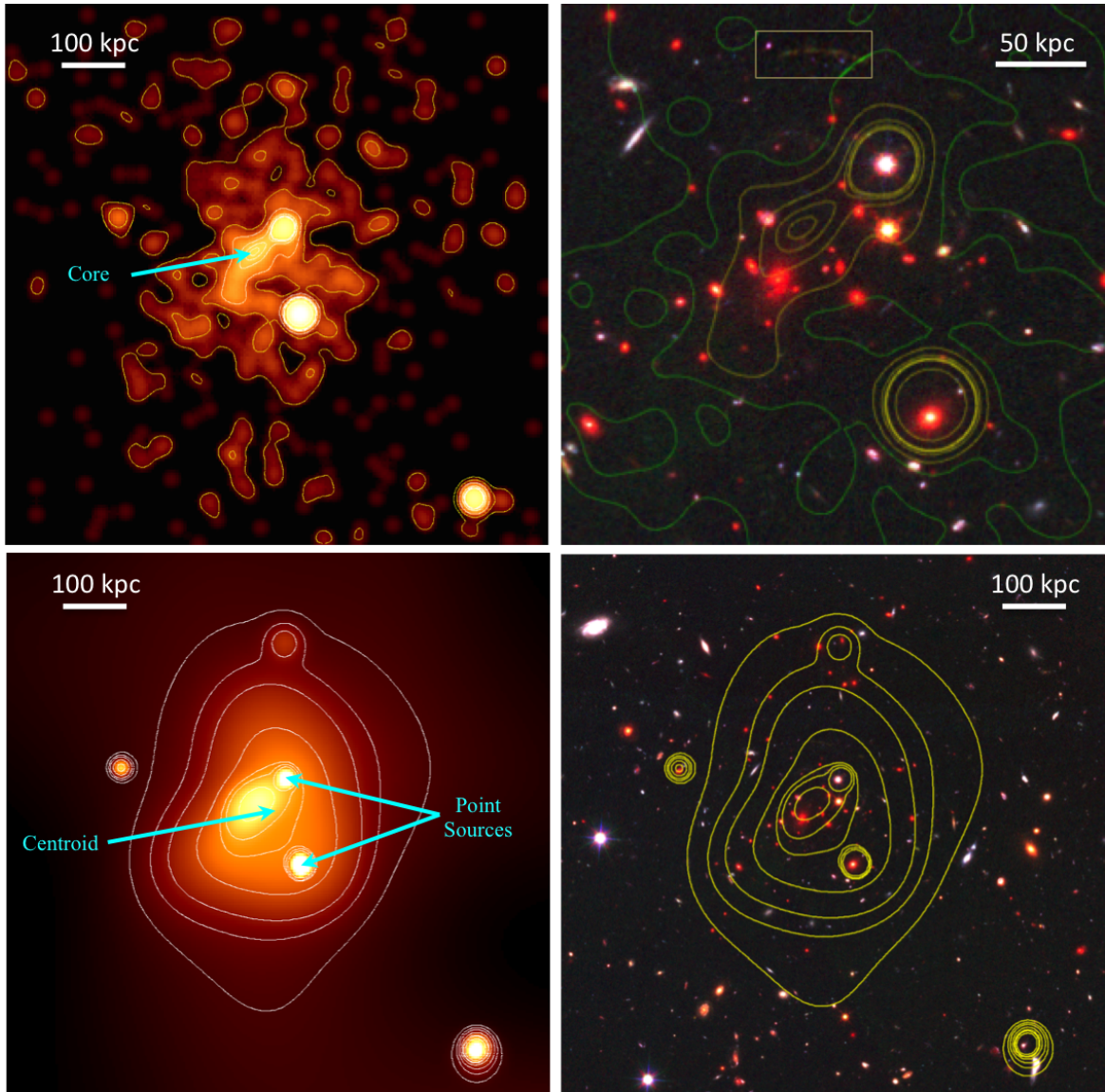


FIG. 1.— *Upper left*: Gaussian-smoothed (FWHM = $3''$) *Chandra* 0.5–2.0 keV image of IDCS J1426.5+3508. Contours correspond to 0.02, 0.05, 0.1, 0.18, 0.22, 0.24, 0.25 and 0.45 counts per $0.492'' \times 0.492''$ pixel. The location of the core as traced by the ICM peak is indicated. *Upper right*: Pseudocolor ACS/F606W, ACS/F814W and WFC3/F160W *HST* image of the central region of IDCS J1426.5+3508, with the X-ray contours from the upper left panel overlaid. The giant arc, boxed, is visible ~ 125 kpc north of the BCG (see Gonzalez et al. 2012). *Lower left*: Adaptively smoothed image of *Chandra* 0.5–2.0 keV image of IDCS J1426.5+3508, showing the large-scale structure from which the cluster centroid was measured. The contours correspond to 0.011, 0.016, 0.022, 0.038, 0.065, 0.085 and 0.15 counts per $0.492'' \times 0.492''$ pixel. The peak emission in the core is offset by ~ 30 kpc from the cluster centroid. Two bright point sources discussed in the text are indicated. *Lower right*: The *HST* image with the same scale and contours as the adaptively smoothed X-ray image.

spectrum using a combination of an absorbed, optically thin plasma (PHABS X APEC), an absorbed hard background component (PHABS X BREMSS; $kT = 40$ keV), and a soft, Galactic background component (APEC; $kT = 0.15$ keV). Foreground and background models were constrained by fitting simultaneously to an off-source region within the same field of view and to the on-source region. The Galactic hydrogen column density, N_{H} , was set to the weighted average from the Leiden-Argentine-Bonn survey (Kalberla et al. 2005). The source redshift was fixed to $z = 1.75$ (Stanford et al. 2012).

The average temperature within r_{2500} is $kT_{2500} = 6.2^{+1.9}_{-1.0}$ keV. This global (not core-excised) temperature, while not optimal as a mass observable due to inclusion of the cluster core, is useful for comparison to lower res-

olution measurements from other facilities or low SNR *Chandra* observations for which all the counts are required to measure the temperature.

We measured the core-excised spectroscopic temperature over $(0.15 - 1) r_{500}$ using the $T_{\text{X}}-M_{500}$ scaling relation from Vikhlinin et al. (2009a) to estimate M_{500} , iteratively updating the radius (r_{500}) until it converged. We used the pipeline described in Benson et al. (in prep.) and McDonald et al. (2013), which closely follows the procedures described in Andersson et al. (2011). We find $kT_{500} = 7.6^{+8.7}_{-1.9}$ keV, in good agreement with the global value given above. This temperature corresponds to a mass of $M_{500, T_{\text{X}}} = 3.3^{+5.7}_{-1.2} \times 10^{14} M_{\odot}$ and $r_{500, T_{\text{X}}} = 560 \pm 20$ kpc, where the subscript refers to the scaling relation from which the physical quantity was de-

rived. The error on the core-excised kT_{500} is larger than that on kT_{2500} as roughly half of the signal is removed with the core, and the noise is significantly increased by moving from r_{2500} to r_{500} .

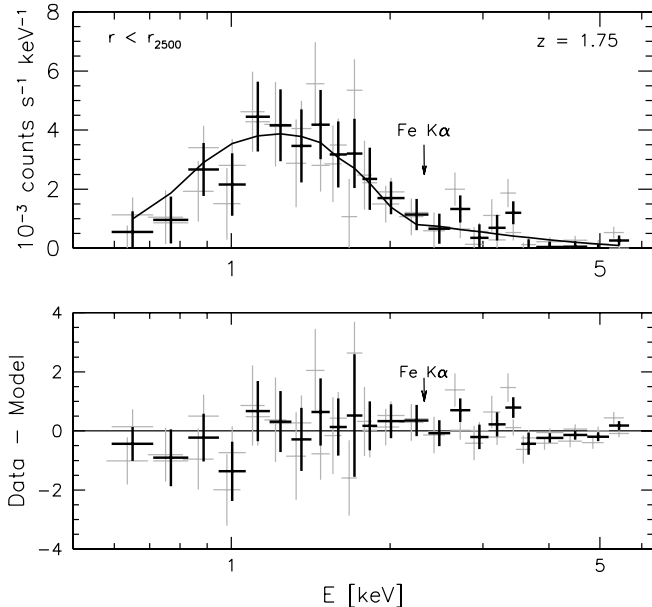


FIG. 2.— *Upper panel:* Energy spectrum of IDCS J1426.5+3508 interior to r_{2500} . The gray points are the two separate observations to which the models are fit, and the black points show the stacked spectrum. The global temperature in this central region, based on the overplotted best-fit model, is $kT_{2500} = 6.2^{+1.9}_{-1.0}$ keV. The expected location of the Fe $K\alpha$ line is indicated, though we do not detect it. The 1σ limit on the central metallicity is $Z_{2500} < 0.33 Z_{\odot}$, as discussed in §3.7. *Lower panel:* Residuals of the best-fit model.

3.5. Gas Mass

Similarly, $M_{g,500}$ was derived via the f_g - M_{500} scaling relation from Vikhlinin et al. (2009a). The derivation of the gas density profile, described in detail in McDonald et al. (2013), involves measuring the X-ray surface brightness in the rest-frame energy 0.7–2.0 keV as a function of radius. The resulting surface brightness profile, shown in Figure 3 (*upper panel*), is fit with a projected double-beta model, following Vikhlinin et al. (2006). In converting from electron density to gas density, we assume $\rho_g = m_p n_e A/Z$, where $A = 1.397$ is the average nuclear charge and $Z = 1.199$ is the average nuclear mass. We integrate the deprojected gas density profile within an initial radius of r_{500, T_x} , estimate the total enclosed gas mass, and then use this to derive M_{500} via the f_g - M_{500} relation. This process is iterated until convergence, leading to a revised estimate of $r_{500, M_g} = 500 \pm 10$ kpc and $M_{500, M_g} = 2.3^{+0.7}_{-0.5} \times 10^{14} M_{\odot}$, consistent with values inferred from the T_X - M scaling relation. The gas mass is $M_{g,500} = 2.5^{+0.8}_{-0.6} \times 10^{13} M_{\odot}$.

3.6. Y_X

The product of the core-excised temperature and gas mass, referred to as Y_X , approximates the total thermal energy in the cluster. It has been shown in simulations to be a low-scatter mass proxy that is independent of

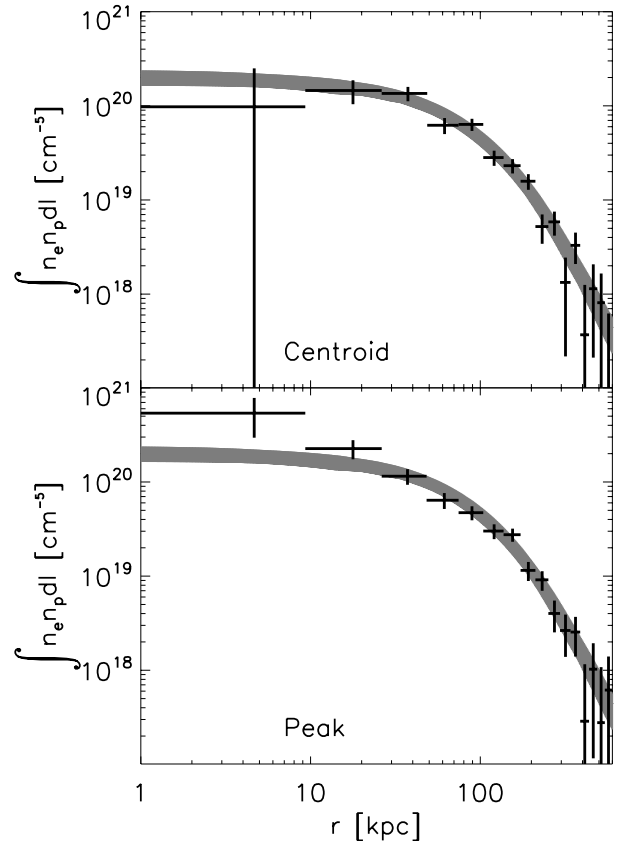


FIG. 3.— *Upper panel:* X-ray surface brightness profile for IDCS J1426.5+3508, derived using the large-scale X-ray centroid as the center. The gray curve represents the best-fit projected double-beta model. *Lower panel:* X-ray surface brightness profile, centered on the X-ray peak. The gray curve is the same as in the upper panel. There is evidence of a dense core on scales of ~ 20 kpc, which appears slightly offset from the large-scale centroid (see Fig. 1).

the dynamical state of the cluster (Kravtsov et al. 2006). Following the same approach as for kT_{500} and $M_{g,500}$, we estimate $Y_{X,500}$ iteratively, adjusting r_{500} to satisfy the Y_X - M_{500} relation. We find $r_{500, Y_X} = 530 \pm 10$ kpc and $M_{500, Y_X} = 2.6^{+1.5}_{-0.5} \times 10^{14} M_{\odot}$. Within r_{500, Y_X} , we measure $Y_{500} = 1.9^{+1.9}_{-0.6} \times 10^{14} M_{\odot} \text{ keV}$.

3.7. Metallicity

Interior to r_{2500} and r_{500} (non core-excised), we measure 1σ (2σ) upper limits on the metallicity of $Z_{2500} < 0.33 Z_{\odot}$ ($0.47 Z_{\odot}$) and $Z_{500} < 0.10 Z_{\odot}$ ($0.18 Z_{\odot}$), respectively. As Figure 2 illustrates, there is no obvious detection of the Fe $K\alpha$ emission line, such that, within r_{2500} , these data are consistent with anywhere from “typical” to a complete absence of metals. Over larger radii we may be observing a marked lack of metals, with the typical average metallicity of low-redshift clusters being $Z_{500} \sim 0.3 \pm 0.1 Z_{\odot}$ (De Grandi and Molendi 2001), a level of enrichment also seen in some $z > 1$ clusters (Rosati et al. 2009; Santos et al. 2012; De Grandi et al. 2014). However, deeper data are needed to properly constrain the metallicity in this system, and determine whether it is, indeed, metal-poor.

TABLE 1
PROPERTIES OF IDCS J1426.5+3508

Property	Value	Unit
z	1.75	
X-Ray Centroid	(14:26:32.6, +35:08:25)	
X-Ray Peak Position	(14:26:32.9, +35:08:26)	
SZ Centroid	(14:26:34.0, +35:08:03)	
BCG Position	(14:26:32.95, +35:08:23.6)	
r_{500, T_x}	560 ± 20	kpc
r_{500, M_g}	500 ± 10	kpc
r_{500, Y_X}	530 ± 10	kpc
Counts	401	
Count Rate	3.95×10^{-3}	s^{-1}
$S_{0.5-2}$	$(2.2 \pm 0.6) \times 10^{-14}$	$\text{erg s}^{-1} \text{cm}^{-2}$
$L_{0.5-2}$	$(3.6 \pm 0.5) \times 10^{44}$	erg s^{-1}
$L_{X, \text{bol}}$	$(12.8 \pm 1.1) \times 10^{44}$	erg s^{-1}
kT_{2500}	$6.2^{+1.9}_{-1.0}$	keV
kT_{500}	$7.6^{+8.7}_{-1.9}$	keV
$M_{g, 500}$	$2.5^{+0.8}_{-0.6} \times 10^{13}$	M_{\odot}
Y_{500}	$1.9^{+1.9}_{-0.6} \times 10^{14}$	$M_{\odot} \text{ keV}$
Z_{2500}	$< 0.33 (1\sigma)$	Z_{\odot}
Z_{500}	$< 0.10 (1\sigma)$	Z_{\odot}
M_{500, Y_X}	$2.6^{+1.5}_{-0.5} \times 10^{14}$	M_{\odot}
M_{500, T_X}	$3.3^{+5.7}_{-1.2} \times 10^{14}$	M_{\odot}
M_{500, M_g}	$2.3^{+0.7}_{-0.5} \times 10^{14}$	M_{\odot}
$M_{500, L_{X, \text{bol}}}$	$(2.8 \pm 0.3) \times 10^{14}$	M_{\odot}
$M_{500, SZ}$	$(2.6 \pm 0.7) \times 10^{14}$	M_{\odot}
$M_{500, \text{arc}}^1$	$(1.9^{+0.7}_{-0.5} - 2.6^{+0.9}_{-0.7}) \times 10^{14}$	M_{\odot}

¹ This mass ranges account for possible sources redshifts between $4.5 < z < 6$, as described in the text.

4. TOTAL MASSES FOR IDCS J1426.5+3508

4.1. M_{500} from X-ray Scaling Relations

Using the measured luminosity, temperature, gas mass and Y_{500} , we reported in the previous section several complementary estimates of the total mass within r_{500} . These masses, along with a host of physical parameters, are listed in Table 1. These masses all show a high level of consistency, indicating IDCS J1426.5+3508 is relaxed, and offering good support for the hydrostatic approximation that is underlying all these scaling relations. A more stringent test is provided by comparisons with complementary, independent mass probes.

4.2. M_{500} from Complementary Measurements

IDCS J1426.5+3508 is unique in that it is the highest redshift cluster, by far, for which independent mass measurements are available in the X-ray, SZ and from strong gravitational lensing analyses. This rare confluence is only possible due to its extreme mass — it is the most massive cluster known at $z > 1.5$ — and the fortuitous (and surprising) presence of a background galaxy for strong lensing (Gonzalez et al. 2012).

Brodwin et al. (2012) reported a strong ($> 5\sigma$) SZ detection at 31 GHz with CARMA. The resulting mass measurement, $M_{500, SZ} = (2.6 \pm 0.7) \times 10^{14} M_{\odot}$, is in excellent agreement with all of the X-ray mass measures presented above. Relative to the Y_{SZ} - M scaling relation from Andersson et al. (2011) that was used in Brodwin et al. (2012), the normalization is expected to increase by $\sim 25\%$ in Y_{SZ} , corresponding to a $\sim 15\%$ increase in mass (Benson et al., in prep.). The increase is primarily due to two factors — a statistical shift resulting from a much

($\sim 5x$) larger SZ and X-ray cluster sample, and updated mass normalization from more recent weak-lensing observations (Hoekstra et al. 2015). The close agreement of the SZ mass for IDCS J1426.5+3508 with the X-ray mass measures will not be affected by this modest change.

Gonzalez et al. (2012) reported the discovery of a giant gravitational arc, visible in Figure 1, about $15''$ N of the BCG at a clustercentric radius of ~ 125 kpc. Attempts to secure a spectroscopic redshift for the source galaxy were unsuccessful, though from the available photometry Gonzalez et al. (2012) constrained the source redshift to the range $2 \lesssim z_s \lesssim 6$. With a non-detection in subsequent deep ($AB \sim 28, 10 \sigma$) *HST*/ACS F606W imaging, new data described in (Mo et al. in prep.), the redshift constraint is now refined to $4.5 \lesssim z \lesssim 6$. The strong lensing mass directly measured within the arc radius ranges from $(6.9 \pm 0.3) \times 10^{13} M_{\odot}$ for $z_s = 6$ to $(8.5 \pm 0.3) \times 10^{13} M_{\odot}$ for $z_s = 4.5$. Extrapolating to r_{500} using the Duffy et al. (2008) mass-concentration relation, this corresponds to a mass range between $M_{500, \text{arc}} = 1.9^{+0.7}_{-0.5} \times 10^{14} M_{\odot}$ and $M_{500, \text{arc}} = 2.6^{+0.9}_{-0.7} \times 10^{14} M_{\odot}$, in good agreement with all the ICM-based masses, particularly for the lower redshift source galaxy.

A weak lensing analysis of IDCS J1426.5+3508 is underway (Mo et al. in prep.). A shear signal is detected in Cycle 20 *HST* images, consistent with expectations for a cluster this massive, even at $z = 1.75$.

Figure 4 (*upper panel*) compares all of the mass measures described in this paper, and shows the uniformly excellent agreement among them. This confirms that, despite its extreme redshift, IDCS J1426.5+3508 is by all measures a relatively evolved, relaxed cluster. We take the low-scatter Y_X -based mass as our best estimate of the halo mass of IDCS J1426.5+3508, $M_{500, Y_X} = 2.61^{+1.22}_{-0.39} \times 10^{14} M_{\odot}$.

4.3. f_{gas}

As massive galaxy clusters assemble, they are expected to retain baryon fractions (f_b) close to (but slightly lower than) the universal value, with relatively low scatter (e.g., Kravtsov and Borgani 2012). Observationally, the gas mass fraction (f_{gas}) is highest in the most massive clusters, with a weakly decreasing fraction to lower masses (e.g., Vikhlinin et al. 2009a; Andersson et al. 2011).

We calculate f_{gas} using each of the masses derived above, integrating the gas mass out to the r_{500} value appropriate to each mass proxy. These are plotted in Figure 4 (*lower panel*). The f_{gas} measurements for which the $M_{g, 500}$ and halo mass measurements are independent are shown as filled symbols, while those affected by covariances between the gas and total mass have open symbols. We compare the measured f_{gas} values with the value predicted from the redshift-independent Andersson et al. (2011) relation. This is shown as the solid red line, where the error range includes the errors from $f_{\text{gas}}-M_{500}$ fit parameters in Andersson et al. (2011), as well as the mass error in M_{500, Y_X} , which we took the value of M_{500} for this relation.

The observed value of f_{gas} from every available mass proxy is completely consistent with the expected value for a cluster with the mass of IDCS J1426.5+3508. This provides additional evidence of the maturity of

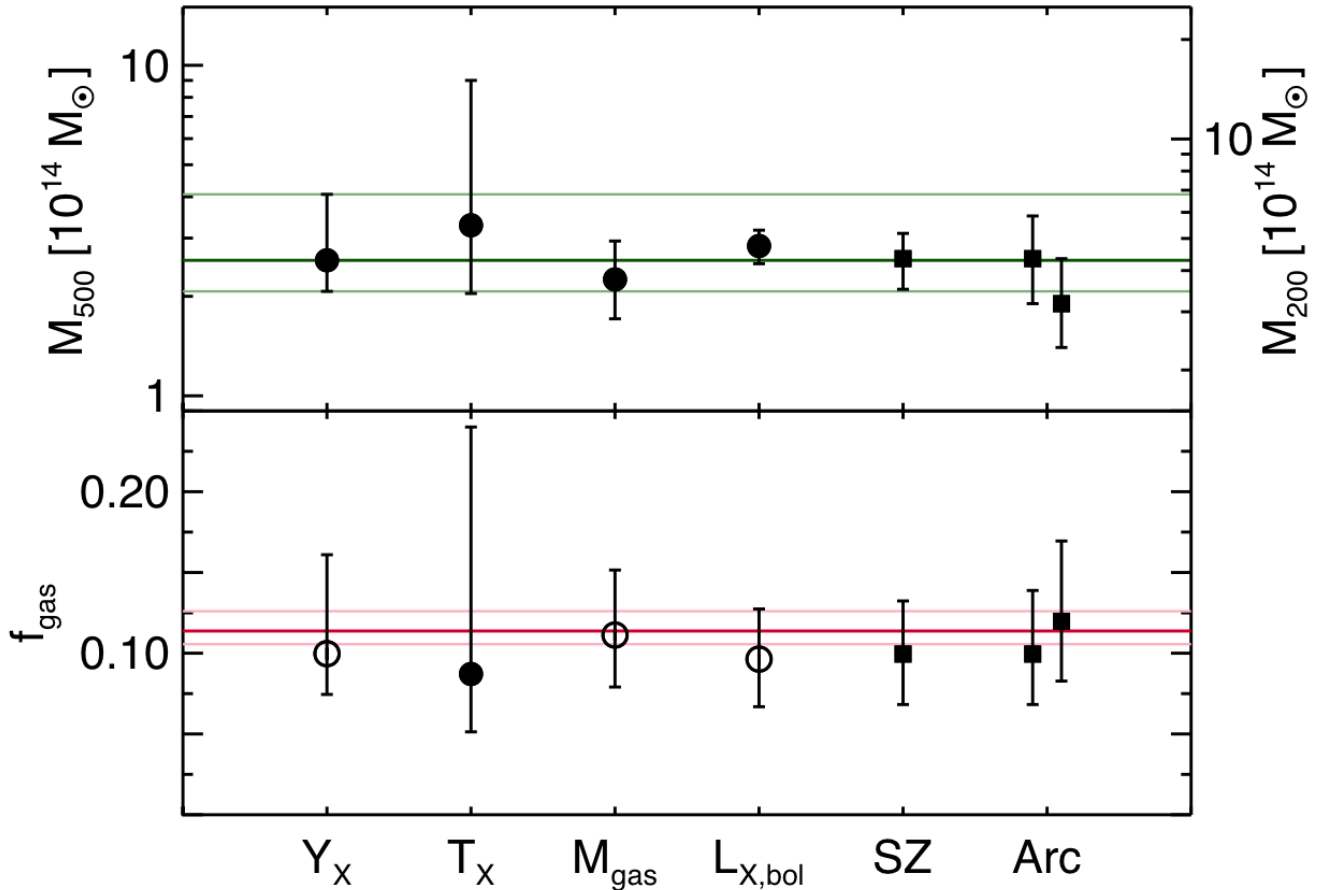


FIG. 4.— *Upper panel:* Masses for IDCS J1426.5+3508 from the X-ray measurements described herein (filled circles), along with complementary SZ (Brodwin et al. 2012) and strong lensing (Gonzalez et al. 2012) masses (filled squares). For the latter we plot the two masses corresponding to the extreme source redshift values, as described in the text. We take the Y_X -based mass our best estimate (green horizontal line and error range), as it has the lowest intrinsic scatter (Kravtsov et al. 2006). The remarkable agreement among these independent methods demonstrates that IDCS J1426.5+3508 is a remarkably mature, evolved cluster even at $z = 1.75$. *Lower panel:* f_{gas} measurements for IDCS J1426.5+3508 using each of these halo mass measurements. f_{gas} measurements with independent $M_{g,500}$ and halo mass measurements have filled symbols; those affected by covariances between the gas and total mass are shown with open symbols. The expected f_{gas} value for IDCS J1426.5+3508, shown as the red line with 1σ errors, is taken from the f_{gas} - M_{500} relation of Andersson et al. (2011). The observed value of f_{gas} is in good agreement with the predicted value for all mass probes.

IDCS J1426.5+3508 and bolsters our confidence in our use of scaling relations at this extreme redshift to estimate its mass.

5. DISCUSSION

5.1. Comparison With Other Distant, Massive Clusters

IDCS J1426.5+3508 was the first relaxed, massive galaxy cluster to be confirmed at $z > 1.5$ (Stanford et al. 2012). The present analysis of its X-ray properties confirms the SZ and lensing masses reported in Brodwin et al. (2012) and Gonzalez et al. (2012), respectively. The former paper also demonstrated that IDCS J1426.5+3508 is an evolutionary precursor to the most massive known clusters at all redshifts. Several new $z > 1.5$ clusters have subsequently been reported, but none are as massive, and hence rare, as IDCS J1426.5+3508. As an illustration of its rarity, consider that although it was selected from the modest 9 deg^2 IDCS area, no clusters as massive at $z > 1.5$ have been confirmed to date within the 2500 deg^2 footprint of the SPT-SZ survey (Bleem et al. 2015), although such clusters would be easily detected by the SPT.

Tozzi et al. (2015) described deep *Chandra* observations of XDCP J0044.0-2033 at $z = 1.58$, from which they measured a total mass of $M_{500, Y_X} = 2.2^{+0.5}_{-0.4} \times 10^{14} M_\odot$, using the same Vikhlinin et al. (2009a) Y_X - M scaling relation employed above. This is below the identical mass measure for IDCS J1426.5+3508, $M_{500, Y_X} = 2.6^{+1.5}_{-0.5} \times 10^{14} M_\odot$, as well as all the other ICM-based (i.e. X-ray and SZ) mass measures in Table 1.

A direct comparison of temperatures is not straightforward, as Tozzi et al. (2015) do not quote a value for T_{2500} or T_{500} . They instead measure a spectroscopic temperature of $kT = 6.7^{+1.3}_{-0.9} \text{ keV}$ at a radius of 375 kpc. As the r_{500} values for both clusters are quite similar, we measure the temperature at this metric radius in IDCS J1426.5+3508 in order to make a meaningful comparison. We find $kT_{375\text{kpc}} = 7.3^{+3.4}_{-2.0} \text{ keV}$, confirming that IDCS J1426.5+3508 is likely the hotter and more massive cluster.

Newman et al. (2014) presented the spectroscopic confirmation of JKCS 041 at $z = 1.80$, for which Andreon et al. (2014) report a mass, based on its X-ray and optical properties, in the range $M_{500} \sim (1-2) \times 10^{14} M_\odot$. Given

the non-detection in deep SZ imaging (Culverhouse et al. 2010), the mass is likely at or below the lower end of that range and thus less massive than IDCS J1426.5+3508.

Finally, cluster candidates reported at $1.6 \lesssim z \lesssim 2$ by Papovich et al. (2010), Zeimann et al. (2012), Gobat et al. (2011, 2013) and Mantz et al. (2014), are all considerably less massive than IDCS J1426.5+3508. Mantz et al. (2014) describe the most massive of these, XLSSU J021744.1-034536 with $M_{500} \sim 1 - 2 \times 10^{14} M_{\odot}$, at a photometric redshift of $z_{\text{phot}} \sim 1.9$. Despite this redshift uncertainty, which strongly affects mass proxies in the X-ray, we can say with certainty that this cluster has a lower mass than IDCS J1426.5+3508. This assertion is based on a comparison of the spherically averaged dimensionless Comptonization, $Y_{\text{sph},500}$, measured with CARMA for both clusters. The SZ mass proxy, $M \propto (Y_{\text{sph},500} D_A^2 / E(z)^{2/3})^{3/5}$ (e.g., Marrone et al. 2012), where D_A is the angular diameter distance and $E(z)$ is evolution of the Hubble parameter, is weakly dependent on redshift. With $Y_{\text{sph},500}$ being a factor of 2.6 higher in IDCS J1426.5+3508, we find its mass is larger by a factor of ~ 1.9 .

5.2. Dynamical and Cooling State of the ICM

In Figure 3 we show the projected surface brightness profile for two different choices of center: the large-scale (250–500 kpc) centroid of the X-ray emission and the X-ray peak. Using the former definition, we fit a projected beta model to the data, finding no evidence for a central surface brightness excess. However, we show in the lower panel of Figure 3 that the peak of the X-ray emission — which lies ~ 30 kpc from the centroid — represents a significant overdensity. Following Vikhlinin et al. (2007), we measure the cuspleness of the peak-centered surface brightness profile, finding $\alpha \equiv (d \log \rho_g / d \log r) |_{0.04 r_{500}} = 0.82 \pm 0.09$. Such a high cuspleness at high redshift is rare. Indeed, Vikhlinin et al. (2007) found no such systems at $z > 0.5$ in their 400 deg² survey. Two similar systems, albeit at much lower redshift ($z \sim 1.1$), have been identified — one by McDonald et al. (2013) in a sample of 83 SPT clusters, and one by Santos et al. (2012) in the WARPS survey.

The offset of ~ 30 kpc between the X-ray centroid and the dense core suggests that this cluster has undergone a recent interaction, and that the cluster core is sloshing about the potential minimum. Such an offset ought to remain visible for $\lesssim 500$ Myr after any interaction (Ascasibar and Markevitch 2006; ZuHone et al. 2010). Considering that this system is being observed when the Universe was only 3.8 Gyr old, and that it had to assemble rapidly to achieve such a high mass at such early times, it is unsurprising that it retains an imprint of this hurried growth in its core.

Following McDonald et al. (2013), we calculate a pseudo-deprojected entropy, using the deprojected gas density profile (§3.5), an aperture temperature, and assuming the X-ray peak as the center. We find $K_0 \sim 20$ keV cm², corresponding to a cooling time of ~ 160 Myr. These properties are typical of cool core clusters (Hudson et al. 2010; McDonald et al. 2013), suggesting that such systems can form very early in the cluster lifetime.

The fact that the dense core appears elongated (Figure 1) suggests that, rather than a traditional cool core, we may be observing a dense infalling group. This is consis-

tent with many of the observed qualities, including the low entropy, the offset from the potential minimum and the non-symmetric morphology. Conversely, the nearly coincident BCG and X-ray peak (within $\sim 3''$; Figure 1) suggests that this may be an offset core rather than an infalling group. Distinguishing between these two scenarios requires a deeper X-ray follow-up observation.

6. CONCLUSIONS

We have presented a deep 100 ks *Chandra* observation of IDCS J1426.5+3508 at $z = 1.75$, the most massive cluster discovered at $z > 1.5$ from *any* method. We measured the luminosity, temperature and gas mass, from which we derived halo mass estimates from the T_X -M, f_g -M, Y_X -M, and L_X -M scaling relations. These all show excellent consistency and are in remarkable agreement with independent SZ and strong lensing masses. Similarly, the gas mass fractions for all these mass proxies were found to be in good agreement with each other and with the value predicted from low redshift clusters.

The bolometric luminosity is $L_{X,\text{bol}} = (12.8 \pm 1.1) \times 10^{44}$ erg s⁻¹, from which we estimate a mass of $M_{500, L_{X,\text{bol}}} = (2.8 \pm 0.3) \times 10^{14} M_{\odot}$. We measure a central temperature within r_{2500} of $kT_{2500} = 6.2^{+1.9}_{-1.0}$ keV and a core-excised temperature within $r_{500, T_x} = 560 \pm 20$ kpc, used in mass scaling relations, of $kT_{500} = 7.6^{+8.7}_{-1.9}$ keV. This results in a mass of $M_{500, T_x} = 3.3^{+5.7}_{-1.2} \times 10^{14} M_{\odot}$. We find no evidence for metals in the ICM of this system, placing a 2σ upper limit of $Z_{500} < 0.18 Z_{\odot}$, suggesting that this system may still be in the process of enriching its intracluster medium.

We measure a gas mass of $M_{g,500} = 2.5^{+0.8}_{-0.6} \times 10^{13} M_{\odot}$, from which we infer an M_g -based halo mass of $M_{500, M_g} = 2.3^{+0.7}_{-0.5} \times 10^{14} M_{\odot}$. From the gas mass and core-excised temperature, we find $Y_{500} = 1.9^{+1.9}_{-0.6} \times 10^{14} M_{\odot}$ keV, from which we derive our lowest-scatter estimate of the mass of IDCS J1426.5+3508, $M_{500, Y_x} = 2.6^{+1.5}_{-0.5} \times 10^{14} M_{\odot}$. All the X-ray masses for IDCS J1426.5+3508 are in agreement, as are the SZ- and lensing-based mass from previous analyses.

The cluster has a dense, low-entropy core, offset by ~ 30 kpc from the X-ray centroid, which makes it one of the few “cool core” clusters discovered at $z > 1$, and the first known cool core cluster at $z > 1.2$. The offset of this core from the large-scale centroid suggests that this cluster has had a relatively recent ($\lesssim 500$ Myr) merger/interaction with another massive system. We measure a central entropy of $K_0 \sim 20$ keV cm², indicating the cool core may have a very rapid cooling time of ~ 160 Myr.

IDCS J1426.5+3508 is the first cluster at $z > 1.5$ to have all these independent mass measurements. In addition to being the most massive known cluster in this redshift regime, IDCS J1426.5+3508 also has a remarkably relaxed ICM suggesting a very early and rapid formation. Deeper follow-up X-ray observations are essential to permit a meaningful constraint on its metallicity and to measure the entropy profile to better understand how and when such cores can form and when the cooling/feedback loop is established.

Support for this work was provided by the National

Aeronautics and Space Administration (NASA) through *Chandra* Award Number GO3-14135A issued the the *Chandra X-ray Observatory* Center, which is operated by the Smithsonian Astrophysical Observatory for and behalf of NASA under contract NAS8-03060. This work is based in part on observations made with the *Spitzer Space Telescope*, which is operated by the Jet Propulsion Laboratory, California Institute of Technology under a contract with NASA. Support for HST programs 11663, 12203 and 12994 were provided by NASA through a grant

from the Space Telescope Science Institute, which is operated by the Association of Universities for Research in Astronomy, Inc., under NASA contract NAS 5-26555.

We thank Alexey Vikhlinin, Bradford Benson and Daniel Marrone for helpful discussions. This paper would not have been possible without the efforts of the support staffs of the *Chandra X-ray Observatory*, and the *Spitzer* and *Hubble Space Telescopes*.

Facilities: Chandra (ACIS-I), HST (ACS, WFC3), Spitzer (IRAC)

REFERENCES

- Andersson, K., et al. 2011, *ApJ*, **738**, 48
 Andreon, S., Newman, A. B., Trinchieri, G., Raichoor, A., Ellis, R. S., and Treu, T. 2014, *A&A*, **565**, A120
 Ascasibar, Y. and Markevitch, M. 2006, *ApJ*, **650**, 102
 Ashby, M. L. N., et al. 2009, *ApJ*, **701**, 428
 Bayliss, M. B., et al. 2014, *ApJ*, **794**, 12
 Becker, R. H., White, R. L., and Helfand, D. J. 1995, *ApJ*, **450**, 559
 Benson, B. A., et al. 2013, *ApJ*, **763**, 147
 Blanton, E. L., et al. 2014, *ArXiv e-prints*
 Bleem, L. E., et al. 2015, *ApJS*, **216**, 27
 Brodwin, M., et al. 2012, *ApJ*, **753**, 162
 Brodwin, M., et al. 2010, *ApJ*, **721**, 90
 Brodwin, M., et al. 2013, *ApJ*, **779**, 138
 Condon, J. J., Cotton, W. D., Greisen, E. W., Yin, Q. F., Perley, R. A., Taylor, G. B., and Broderick, J. J. 1998, *AJ*, **115**, 1693
 Culverhouse, T. L., et al. 2010, *ApJ*, **723**, L78
 De Grandi, S. and Molendi, S. 2001, *ApJ*, **551**, 153
 De Grandi, S., Santos, J. S., Nonino, M., Molendi, S., Tozzi, P., Rossetti, M., Fritz, A., and Rosati, P. 2014, *A&A*, **567**, A102
 Duffy, A. R., Schaye, J., Kay, S. T., and Dalla Vecchia, C. 2008, *MNRAS*, **390**, L64
 Eisenhardt, P. R., et al. 2004, *ApJS*, **154**, 48
 Eisenhardt, P. R. M., et al. 2008, *ApJ*, **684**, 905
 Fassbender, R., et al. 2011, *New J. Phys.*, **13**, 125014
 Foley, R. J., et al. 2011, *ApJ*, **731**, 86
 Gobat, R., et al. 2011, *A&A*, **526**, A133
 Gobat, R., et al. 2013, *ApJ*, **776**, 9
 Gonzalez, A. H., et al. 2012, *ApJ*, **753**, 163
 Hasselfield, M., et al. 2013, *JCAP*, **7**, 8
 Hilton, M., et al. 2010, *ApJ*, **718**, 133
 Hoekstra, H., Herbonnet, R., Muzzin, A., Babul, A., Mahdavi, A., Viola, M., and Cacciato, M. 2015, *MNRAS*, **449**, 685
 Hudson, D. S., Mittal, R., Reiprich, T. H., Nulsen, P. E. J., Andernach, H., and Sarazin, C. L. 2010, *A&A*, **513**, A37
 Kalberla, P. M. W., Burton, W. B., Hartmann, D., Arnal, E. M., Bajaja, E., Morras, R., and Pöppel, W. G. L. 2005, *A&A*, **440**, 775
 Kravtsov, A. V. and Borgani, S. 2012, *ARA&A*, **50**, 353
 Kravtsov, A. V., Vikhlinin, A., and Nagai, D. 2006, *ApJ*, **650**, 128
 Mancone, C. L., Gonzalez, A. H., Brodwin, M., Stanford, S. A., Eisenhardt, P. R. M., Stern, D., and Jones, C. 2010, *ApJ*, **720**, 284
 Mantz, A. B., et al. 2014, *ApJ*, submitted (arXiv:1401.2087)
 Marrone, D. P., et al. 2012, *ApJ*, **754**, 119
 Marshall, H. L., Tennant, A., Grant, C. E., Hitchcock, A. P., O'Dell, S. L., and Plucinsky, P. P. 2004, in K. A. Flanagan and O. H. W. Siegmund (eds.), *X-Ray and Gamma-Ray Instrumentation for Astronomy XIII*, Vol. 5165 of *Society of Photo-Optical Instrumentation Engineers (SPIE) Conference Series*, pp 497–508
 McDonald, M., et al. 2013, *ApJ*, **774**, 23
 Mehrrens, N., et al. 2012, *MNRAS*, **423**, 1024
 Muzzin, A., et al. 2009, *ApJ*, **698**, 1934
 Newman, A. B., Ellis, R. S., Andreon, S., Treu, T., Raichoor, A., and Trinchieri, G. 2014, *ApJ*, **788**, 51
 O'Dell, S. L., Swartz, D. A., Tice, N. W., Plucinsky, P. P., Grant, C. E., Marshall, H. L., Vikhlinin, A., and Tennant, A. F. 2013, in *Society of Photo-Optical Instrumentation Engineers (SPIE) Conference Series*, Vol. 8859 of *Society of Photo-Optical Instrumentation Engineers (SPIE) Conference Series*, p. 0
 Papovich, C., et al. 2010, *ApJ*, **716**, 1503
 Planck Collaboration, Ade, et al. 2015, *A&A*, submitted (arXiv:1502.01598)
 Pratt, G. W., Croston, J. H., Arnaud, M., and Böhringer, H. 2009, *A&A*, **498**, 361
 Rettura, A., et al. 2014, *ApJ*, **797**, 109
 Rosati, P., et al. 2009, *A&A*, **508**, 583
 Santos, J. S., Tozzi, P., Rosati, P., Nonino, M., and Giovannini, G. 2012, *A&A*, **539**, A105
 Stalder, B., et al. 2013, *ApJ*, **763**, 93
 Stanford, S. A., et al. 2012, *ApJ*, **753**, 164
 Tozzi, P., et al. 2015, *ApJ*, **799**, 93
 Tran, K., et al. 2010, *ApJ*, **719**, L126
 Vikhlinin, A., Burenin, R., Forman, W. R., Jones, C., Hornstrup, A., Murray, S. S., and Quintana, H. 2007, in H. Böhringer, G. W. Pratt, A. Finoguenov, and P. Schuecker (eds.), *Heating versus Cooling in Galaxies and Clusters of Galaxies*, p. 48
 Vikhlinin, A., et al. 2009a, *ApJ*, **692**, 1033
 Vikhlinin, A., Kravtsov, A., Forman, W., Jones, C., Markevitch, M., Murray, S. S., and Van Speybroeck, L. 2006, *ApJ*, **640**, 691
 Vikhlinin, A., et al. 2009b, *ApJ*, **692**, 1060
 Vikhlinin, A., McNamara, B. R., Forman, W., Jones, C., Quintana, H., and Hornstrup, A. 1998, *ApJ*, **502**, 558
 Wylezalek, D., et al. 2013, *ApJ*, **769**, 79
 Zeimann, G. R., et al. 2012, *ApJ*, **756**, 115
 Zuhone, J. A., Markevitch, M., and Johnson, R. E. 2010, *ApJ*, **717**, 908